Scientific Research Publishing

Open Journal of Ophthalmology, 2026, 16(1), 12-25
https://www.scirp.org/journal/ojoph
ISSN Online: 2165-7416
ISSN Print: 2165-7408

Anatomical Modeling for the Validation of Automated Measurement of the Angle of Deviation in the Strabismic Head Model

Jack Berglas[1], Arpine Rostomyan[2], Armen Sargsyan[3], Ara Keshishian[4*]

[1]Department of Engineering, Orange Coast College, Costa Mesa, CA, USA
[2]Department of Medicine, Virginia Commonwealth University School of Medicine, Richmond, VA, USA
[3]Human Psychophysiology Laboratory, Orbeli Institute of Physiology, Yerevan, Armenia
[4]Department of Surgery, Verdugo Hills Hospital, University of Southern California, Glendale, CA, USA
Email: *ara.keshishian@med.usc.edu

How to cite this paper: Berglas, J., Rostomyan, A., Sargsyan, A. and Keshishian, A. (2026) Anatomical Modeling for the Validation of Automated Measurement of the Angle of Deviation in the Strabismic Head Model. *Open Journal of Ophthalmology*, **16**, 12-25.
https://doi.org/10.4236/ojoph.2026.161002

Received: November 13, 2025
Accepted: December 27, 2025
Published: December 30, 2025

Abstract

Purpose: Angle of Deviation (AOD) and Prism Diopter (PD) measure the relative deviation between the eyes. Many conditions can cause misalignment of the eyes (Strabismus) and result in reduced visual acuity in one eye (Amblyopia). Misalignment may be observed in children; for most, it is self-limiting. However, some may develop strabismus, which, if left uncorrected, can lead to amblyopia and loss of peripheral vision and depth perception. Clinical examination for accurate measurement of eye alignment is highly technical and prone to variations and inaccuracies. In the absence of a validated testing platform, the clinical measurement has been used as the standard measurement. Our model provides a validated tool for calibration and accurate measurement of AOD and PD. **Method:** The application developed measures the eye alignment. We designed 3D-printed full-scale anatomical heads with interchangeable eye inserts that feature deviations in precise pupil position in both the horizontal and vertical planes. The application's measurement was validated by evaluating the deviation of the 3D head model printed with precisely known variations. **Results:** Using the model created, we validated precise AOD and PD measurements with our app, PinpointEyes APP, as predicted by the mathematical models. **Conclusion:** The PinpointEyes 3D Model (PPEM) is an accurate platform that validates the AOD and PD measurements in research protocols. This provides a pathway to establish the standard for the precise measurement of AOD and PD. **Translational Relevance:** The model developed serves as a validation platform for the accurate measurement of PD and AOD.

Keywords

Angle of Deviation, Prism Diopter, Strabismus, Modeling

1. Introduction

Prism Diopter is a clinical measurement used to quantify the AOD of the eyes, dating back to its origin in the late 1870s. [1] One PD (1Δ) is defined as the bending of the beam of light by 1 cm toward the base of a prism 100 cm from the prism.

Accurate PD measurement depends heavily on the examiner's experience and the patient's cooperation. [2] Possible sources of error in PD measurement include patient compliance, examiner experience, stability, and the parallel orientation of the prism to the subject's eyes. [3] As measured PD increases, the difference between repeated measurements increases, raising questions about the validity of large-angle PD values. [4] Even minor measurement errors result in significant planned operative variation. [5]

Applications for smartphones and tablet devices have been developed to measure the angle of deviation and report a calculated PD. The comparative value of these has been based on mathematical modeling that references clinical PD measurements. [6] We have previously reported on our research, both in adults and in children, comparing clinical PD measurements with results from the PinpointEyes App (PPEA). [3] [7] The principal premise of the published data is that PD measurements obtained with devices should be compared against clinical PD measurements. This assumes that the clinical PD measurements are accurate and reproducible and serve as the reference point against which all measurements are evaluated—a position not supported by the literature. [2] [8] [9] We have developed a precise testing platform to validate PPEA measurements and the calculated PD results. The designed 3-D model of an adult human head with known deviations in the eye inserts allows us to confirm the algorithm's reported PD using a precise, known model.

2. Physiology

The process of seeing and perceiving an object begins as light rays reflect off an object and enter the eyes. The light then passes through the pupil, controlled by the surrounding-colored muscle, the iris, which adjusts pupil size to control the amount of light that enters the retina. [10] Two types of photoreceptors, cones and rods, convert light information into electrochemical signals when light hits the retina. [11]

Information from the left visual field activates the nasal retina of the left eye and the temporal retina of the right eye. [12] In contrast, information from the right visual field similarly activates the opposite regions. The upper and lower quadrants of the visual field correspond to the upper and lower areas of the retina, respectively. [13] The horizontal separation of the eyes creates differences in the images received by each retina. This results in two different but similar images that the brain processes, creating a phenomenon known as binocular disparity, which is imperative for depth perception. The image produced on the retina and perceived in the visual cortex involves the brain's ability to merge two similar yet non-overlapping images. [14] This image processing at the brain level is crucial

for depth perception and a nearly 180-degree field of vision. If the eyes are misaligned in the same gaze direction, the signals will fail to merge into a three-dimensional image. [15] Depth perception and three-dimensional visualization occur when the brain integrates images from both eyes.

Patients with strabismus experience difficulties with depth perception because the brain suppresses visual stimuli from the misaligned eye to prevent double vision. Similarly, stroke damage to the visual cortex or dorsal pathway regions interferes with depth perception and spatial orientation, despite intact eyes and optic nerve structures. [16]

3. Visual Testing

Hirshberg, Modified Krimsky, and Prism Cover tests are clinical examinations that assess AOD and PD. The accuracy of these tests largely depends on each examiner's experience. [17] Significant limitations exist in a specific test: repeated examinations of the same subject over a very short period by the same examiner can yield results that may vary considerably. [18] [19] These variations cannot be attributed to fundamental changes in AOD or PD, particularly concerning minor differences. However small, this measurement is critical in planning corrective eye surgeries.

These tests' limitations stem from the human factor involved in taking the measurements. The tests depend on the examiner's estimation and observation, as well as the patient's cooperation. [2] These human variables make the validity and reproducibility of these tests unreliable in pediatric patients and those who cannot follow instructions due to age or health conditions.

There may be several reasons for the non-reproducibility and variability of clinical PD measurement. [9] PD measurement is highly dependent on the examiner's experience. [17] The results of the PD test are influenced by several variables, including the examiner's position, the patient's proximity, the prism's position relative to the patient's eye, and the distance measured. [19] The examiner may not be able to control some of these variables, given the patient's very young age and inability to follow instructions, hold still, or both. The initial and repeated PD tests (one hour apart) at near and distance resulted in exact measurements in only 37% and 53% of cases, respectively. [4]

Given the broad variability in repeated testing, regardless of potential causes, one can question the validity and reliability of the PD test, since this measurement, along with other variables, is used to plan and execute the surgical approach to strabismus surgery with muscle repositioning. [20] [21]

4. Application Design

With the current Smartphone Apps, we have identified several deficiencies. Firstly, several smartphone devices have been reported to measure AOD and PD using various techniques, which may require expert training in a clinical setting and are not tested or suited for broad use in primary care or at home. [22] [23] Secondly,

they validate their results against a clinician's examination, which shows wide examiner-dependent variability. [5] [24] A smartphone device should be validated on a standardized testing platform that allows reproducibility within and across repeated examinations by different operators and smartphones.

Our solution consisted of design validation process. The first step involved modeling and 3D printing an anatomically accurate human head. A head with changeable eyes at known offsets was needed to validate measurements made by the PPEA. The test platform needed to have: 1-known tolerances to allow for precise measurement, and 2-precise offsets to ensure the measurements taken from the app could be trusted in real-world applications. Our model was built on an open-source design using computer-aided design (CAD). The optimization included exchangeable eye inserts (EEI) with different iris-pupil positions. The 3D-printed head and a series of EEIs with varying angles of deviation would enable us to model the deviated eye position at a known, precise angle. All variables- the radius of the eye and deviation in arc millimeters on horizontal and vertical planes- were established to have less than one-millimeter tolerance.

The second step used the PinpointEyes app (PPEA) to measure AOD and PD with both the non-deviated and deviated EEIs. This allowed us to verify the PPEA-reported data by confirming the accuracy of measurements against the expected values obtained during model creation in the second step.

This structured and systematic approach results in a reliable, easy-to-use, data-driven testing platform for measuring AOD and PD, accurate across all smartphones and users, using a "point and take picture" approach.

5. Design Process

5.1. Design of the Head

The design of the head began by resizing an open-source design to specific dimensions within the range of average human facial measurements. Further additions included recessed and protruded lines along the center of the face for precise positioning, a calibration 1cm square above the bridge of the nose, and Interchangeable eyes for straight and deviated gaze positions.

The design included the following parameters:

a) The pupil's diameter was set to 2 mm (ref), and the complete set of eyes was printed for both the left and right sides.

b) Both sets also included inward (esotropia) and outward (Exotropia) deviation.

c) Horizontal deviated positions were at 2-millimeter increments.

d) The curvature of the visible part of the eyes is based on an average eye diameter of 1.125 cm (ref).

e) Design measurements are printed on the back of the head.

5.2. Design of Exchangeable Eye Inserts (EEI)

For the horizontal deviation, each set consists of 8 inserts per side in both inward

(esotropia) and outward (exotropia) deviation, with deviation set in the horizontal plane from the central pupil position (+2 mm, +4 mm, +6 mm, +8 mm, −2 mm, −4 mm, −6 mm, −8 mm). For the Vertical deviation, each set consists of 4 inserts per side, in both inward (esotropia) and outward (Exotropia) deviation, with deviation set in the horizontal plane from the central pupil position (+2 mm, +4 mm, −2 mm, −4 mm).

Two additional EEIs are made for full deviation to the inner and outer Canter positions (with the whole pupil visible). The deviations are set as Arc distance on the surface of the eye. Two complete sets of the EEIs mentioned above were printed, with pupil bores to accommodate both LED lights. The distance between pupils was set at 60 mm.

This translates to the following measurements outlined in the addendum "IC_OC Offset Dimensions.xlsx".

5.3. 3D Printing

The printer used for this project was a Creality Ender 3 (https://www.creality.com/), running its stock Marlin firmware (tolerances of ±0.1 mm, 0.4 mm nozzle, height 0.16 mm). A direct-drive extruder replaced the stock Bowden setup, improving filament control, precision, and material versatility. The bed was also upgraded to a glass plate, providing a flat, smooth surface that improves adhesion and consistency. All modeling for this project was performed using Autodesk Fusion 360 (V. 2.0.20508) and Ultimaker Cura under an educational license.

6. Method: Setup and Procedure

Using the Pinpoint Eyes smartphone application, we measured the Angle of Deviation (AOD) and Prism Diopter (PD) values from images of a 3D-printed anatomical head with preset pupil deviations, simulating varying eye deviation. The application was used to process the images and calculate the AOD and PD values. These values were compared with the known parameters and analyzed for statistical significance to evaluate the program's efficacy.

The 3-D model was custom-engineered to feature interchangeable eye inserts with pre-defined horizontal pupil deviations. The inserts were designed to represent known displacements of the right and left pupils from a central position (0mm). These included displacements of 2 mm, 4 mm, 6 mm, and 8 mm from the center, both toward the inner canthus (labeled with a negative sign, −2mm, 4 mm, etc.) and outer canthus (labeled with a positive sign: +2 mm, +4 mm, etc.). Additionally, inserts were created to represent complete deviations toward the inner and outer canthi (labeled as 1.0 I.C., 1.0 O.C., respectively), as well as half displacements between the central position (0 mm) and the inner or outer canthus (labeled as 0.5 I.C., 0.5 O.C., respectively) (**Figure 1**).

Figure 2 shows a non-deviated eye insert, and **Figure 3** shows a left 8mm deviation.

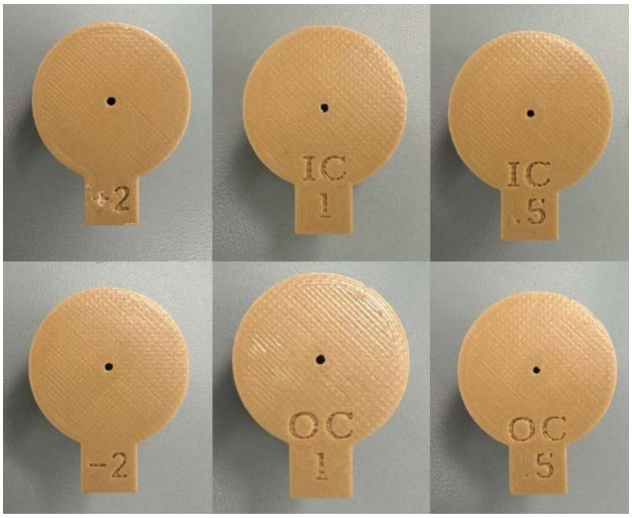

Figure 1. Deviated eye inserts marked with position information.

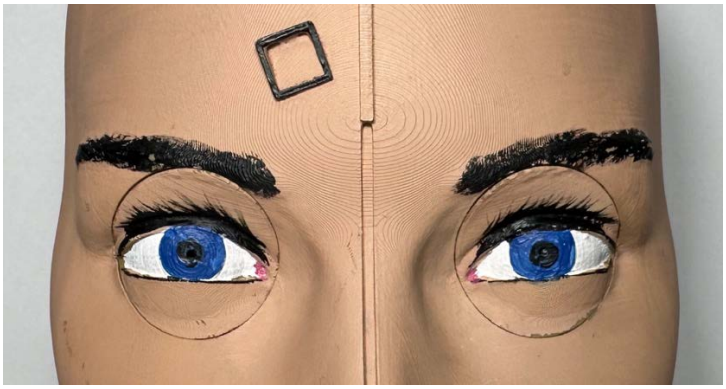

Figure 2. Non-deviated eye insert.

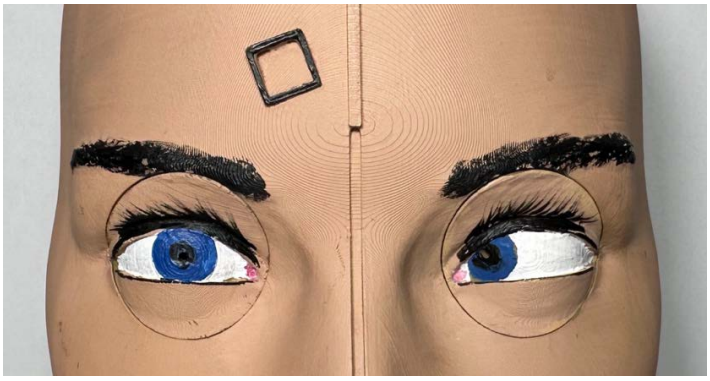

Figure 3. Left 8 mm—horizontal only deviated eye insert.

The anatomical model was secured onto a 3-D printed tailored platform with a rotating hook mechanism, allowing rotation of the anatomical head about the z-axis in 5˚ increments, ranging from 0˚ (centered) to ±45˚ (clockwise and counter-clockwise). Two additional spirit levels were attached to the posterior of the head model, ensuring the model is aligned vertically and horizontally along the y and

x-axes, respectively (Figure 4).

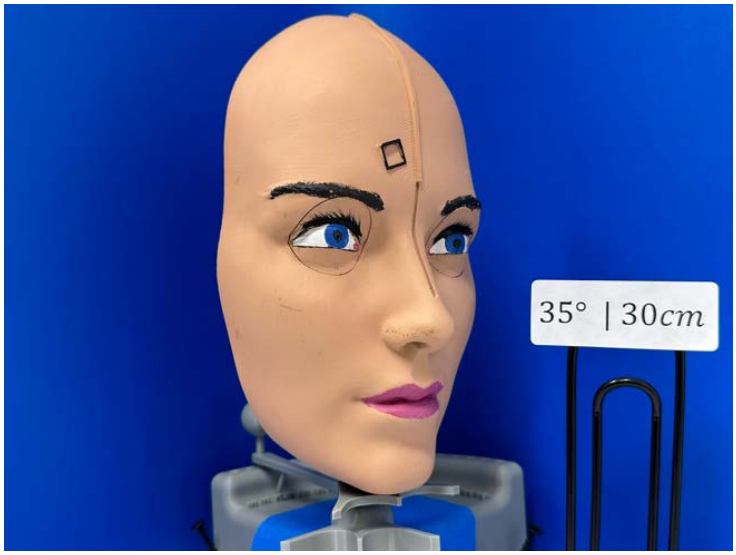

Figure 4. 3-D printed head with eye insert, on the rotating platform.

Photographs of the model were taken using an iPhone 13 Pro. The camera was configured to standard mode throughout the image collection. The device was secured on a fixed tripod stand with three spirit levels mounted to the iPhone case, enabling control of the x- and y-axis tilt (Figure 5). A needle was centrally positioned between the iPhone's three rear-facing camera lenses and used to precisely align the camera with pre-defined coordinates on a gridded platform beneath the setup. The grid paper was labeled with distance and angular markers to help standardize the distance between the camera and model across trials. Images were captured at four distances from the model: 45 cm, 40 cm, 35 cm, and 30 cm. The phone stand and model were outlined on the grid paper after each repositioning to minimize inconsistencies across image sets.

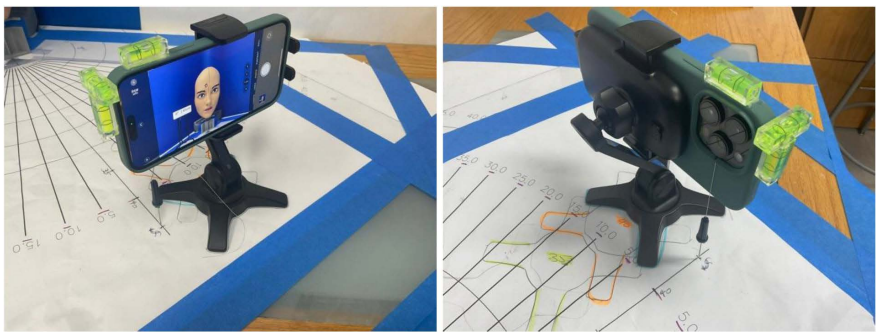

Figure 5. Multi-axis tripod setup.

For image sets collected at 45 cm, 40 cm, and 35 cm, 1.4× digital magnification was applied; for images captured at 30 cm, a 1.1× magnification was used. Utilization of the magnification feature automatically engaged the iPhone's Telephoto lens

(equivalent focal length: 77 mm). All images were recorded in landscape orientation at a resolution of 4032 × 3024 pixels. Lighting conditions were controlled by manually adjusting focus and exposure before each image was captured. The Live Photo feature was enabled to allow for automatic minor post-processing adjustments.

A standardized data-collection protocol was developed. Images were captured for each deviation setting across all rotation angles and distances and labeled accordingly. The head was then rotated with the same eye insert in 5˚ increments clockwise and counterclockwise, up to 45˚, with cautious re-leveling after each adjustment. Collection for the insert with the same rotation adjustments was repeated at distances of 30 cm, 35 cm, 40 cm, and 45 cm. Photograph series were captured identically for each eye insert, representing a unique deviation setting.

The image collection was uploaded to the application in a single batch to calculate the AOD and PD values. Images were manually processed by standardly marking each eye's inner and outer canthi, iris center, the iris inner and outer edge, and the center point along the nasal dorsum that aligns with the iris centers of both eyes. The software calculated the AOD and (PD) values as described below. The comprehensive dataset was compared to the head model's known measurements and evaluated for statistical significance.

7. Method: The AOD and PD Calculation

The image may be tilted in the coronal plane, and the deviated eye is known (left or right). The following image points are provided: the pupil centers, and either the outer or the inner canthi. We assume that the non-deviated (normal) eye looks straight ahead (**Figure 6(A)**).

First, the linear disposition of the deviated eye along the tilted X and Y axes compared to the non-deviated eye, Δx and Δy, is calculated as differences between distances of the pupil centers of deviated (dxD) and non-deviated (dxN) eyes and a face centerline:

$$\Delta x = dxD - dxN,\ \Delta y = dyD - dyN, \tag{1}$$

where

$$dxD = dx_R,\ dyD = dy_R;\ dxN = dx_L,\ dyN = dy_L, \text{ (right eye deviation)}, \tag{2}$$

or

$$dxD = dx_L,\ dyD = dy_L;\ dxN = dx_R,\ dyN = dy_R, \text{ (left Eye deviation)}. \tag{3}$$

The tilted X axis is defined by the equation of a line connecting two given points, the left and right eyes' outer (or inner) canthi, (x_L, y_L) and (x_R, y_R):

$$\frac{x - x_L}{x_R - x_L} = \frac{y - y_L}{y_R - y_R}.$$

The tilted Y axis is defined as perpendicular to the X axis.

Then dy_L and dy_R can be found as distances from the pupil centers to the X axis:

$$dy_L = \frac{\left|\left(x_R - x_L\right)\left(y_L - y_{CL}\right) - \left(x_L - x_{CL}\right)\left(y_R - y_L\right)\right|}{\sqrt{\left(x_R - x_L\right)^2 + \left(y_R - y_L\right)^2}},$$

$$dy_R = \frac{\left|(x_R - x_L)(y_L - y_{CR}) - (x_L - x_{CR})(y_R - y_L)\right|}{\sqrt{(x_R - x_L)^2 + (y_R - y_L)^2}}.$$

To find the dx_L and dx_R, we first define a center point as follows:

$$x_0 = \frac{x_R - x_L}{2} + x_L, y_0 = \frac{y_R - y_L}{2} + y_L.$$

We then find the distances from the center point to pupil centers:

$$c_L = \sqrt{(x_{CL} - x_0)^2 + (y_{CL} - y_0)^2},$$

$$c_R = \sqrt{(x_{CR} - x_0)^2 + (y_{CR} - y_0)^2}.$$

Finally, from the right triangle formula, we find dx_L and dx_R:

$$dx_L = \sqrt{c_L^2 - dy_L^2},$$

$$dx_R = \sqrt{c_R^2 - dy_R^2}.$$

Then Δx and Δy are determined using (1), (2), and (3) for the correct deviated eye.

Knowing Δx and Δy and the eyeball radius R, we can calculate the AODs for the X and Y axes as

$$\alpha_x = \arcsin(\Delta x / R),$$

$$\alpha_y = \arcsin(\Delta y / R).$$

The eyeball radius, R, is maintained constant in millimeters (**Figure 6(B)**). In our 3D-printed head, the eyeball radius is 12.25 mm, consistent with the literature. [25] Iris diameter in the image, which is also known and varies insignificantly among individuals. [26] [27] In our 3D-printed head, the iris diameter is 11.5 mm.

The iris diameter in pixels can be calculated from the edge points (x_1, y_1) and (x_2, y_2) of the iris (**Figure 6(C)**):

$$\boldsymbol{d_{iris}} = \sqrt{(\boldsymbol{x}_2 - \boldsymbol{x}_1)^2 + (\boldsymbol{y}_2 - \boldsymbol{y}_1)^2}$$

The iris diameters are measured for both eyes, and the average is calculated.

Knowing the iris diameter in pixels and in mm, we can then calculate the scaling factor for conversion from pixels to mm as

$$s = d_{iris} / 11.5.$$

We then convert the eyeball radius from mm to pixels:

$$R_{pix} = 12.25 \times s,$$

and calculate the AODs as

$$\alpha_x = \arcsin(\Delta x / R_{pix}),$$

$$\alpha_y = \arcsin(\Delta y / R_{pix}).$$

The PD will then be:

$$PD_x = 100 \tan \alpha_x ,$$

$$PD_y = 100 \tan \alpha_y .$$

Automatic detection of the deviated eye.

The deviated eye is determined by estimating the asymmetry of each eye. The asymmetry of the eyes in pixels is defined as:

$$A_{Rpix} = \left| dx_{OR} - dx_{IR} \right| ,$$

$$A_{Lpix} = \left| dx_{OL} - dx_{IL} \right| ,$$

where

$dx_{OR} = x_{CR} - x_{OR}$ is the distance between the right iris center and the right outer canthus,

$dx_{IR} = x_{IR} - x_{CR}$ is the distance between the right inner canthus and the right iris center,

$dx_{OL} = x_{OL} - x_{CL}$ is the distance between the left outer canthus and the left iris center,

$dx_{IL} = x_{CL} - x_{IL}$ is the distance between the left iris center and the left inner canthus.

A_{Rpix} and A_{Rpix} are then normalized by dividing by the iris diameter:

$$A_{Rnorm} = A_{Rpix} / d_{iris}$$

$$A_{Lnorm} = A_{Lpix} / d_{iris} .$$

The eye with greater normalized asymmetry is the deviated eye.

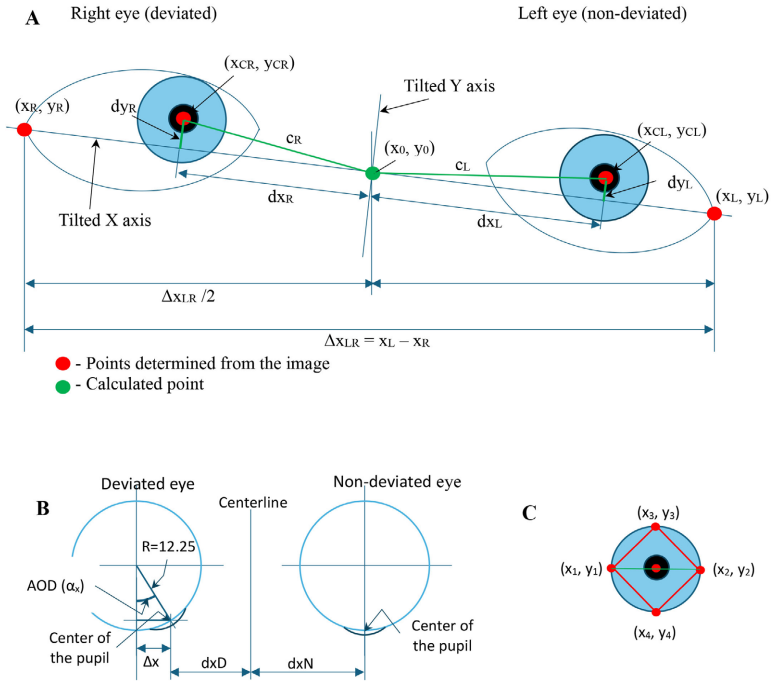

Figure 6. (A) Schematic representation of the eyes on an image with a slightly tilted face, coronal plane. In this example, the deviated eye is the right eye. (B) Schematic representation of eyeballs in the transverse plane. (C) The iris diameter.

8. Validation

The 3D model and PPEA accuracy were validated by taking pictures with an iPhone 13 Pro (4032 × 3024 pixels) and loading the images into the app from the photo library. To avoid examiner bias, one image was taken without a label, and a second was taken with the deviation label (Figure 7). They were then loaded into the PPEA by two research associates, and the outcomes were recorded (Table 1). Using a paired two-tailed t-test, the difference between the 3-D model PD and the measured PPEA PD for both ESO and EXO was not statistically significant (P = 0.46762).

Table 1. 3D model and PPEA Prism diopter measurements.

No	Eye	Label	Deviation (mm)	Calculated angle	Calculated Prism diopter δ(Δ)	PPEA Measured angle	PPEA Measured Prism diopter δ(Δ)	Diff. Angle	Diff. diopter δ(Δ)
1	R	0	0	0	0	1	1	#DIV/0!	#DIV/0!
2	R-EXO	2	2	9	16	10	18	10%	10%
3	R-EXO	4	4	19	34	19	35	3%	3%
4	R-EXO	6	6	28	53	27	51	5%	−5%
5	R-EXO	8	8	37	77	36	72	4%	−6%
6	R-ESO	-2	2	9	16	10	17	6%	6%
7	R-ESO	-4	4	19	34	19	35	3%	3%
8	R-ESO	-6	6	28	53	29	55	3%	3%
9	R-ESO	-8	8	37	77	33	65	12%	−15%

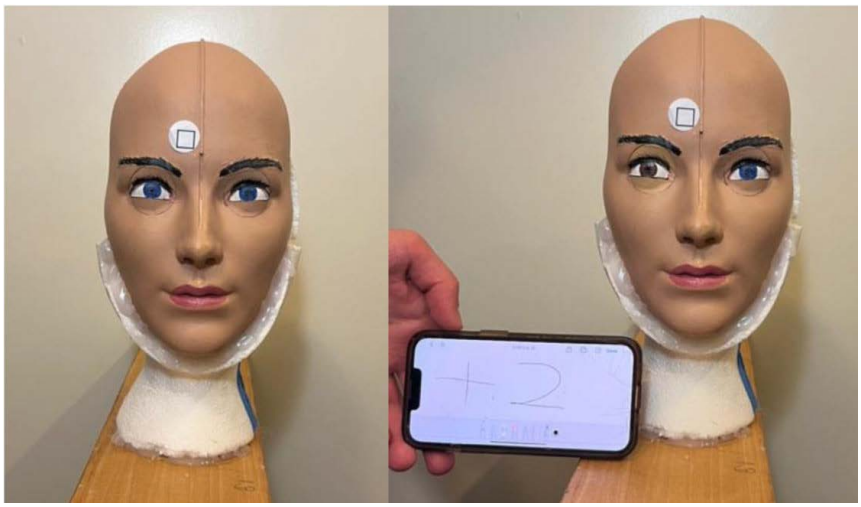

Figure 7. Examples of non-labeled and labeled images.

9. Summary

We have built a 3-D model to accurately validate AOD and PD measurements obtained with a mobile app. This model can serve as the gold standard for measuring AOD and PD when evaluating the accuracy, reproducibility, and predictability of those measurements in a clinical setting.

Repository

The supplemental information is stored in the GitHub repository:
https://github.com/hyperionlaboratories/3D-Validation-publication

Ethical, Funding, and Financial Disclosure

This research was conducted in accordance with ethical standards and did not involve any human or animal subjects. All work and analyses were completed independently, with no external funding or financial contributions exchanged. Armen Sargsyan, PhD, Jack Berglas, and Andranik Sinanyan are contracted consultants of the project. Ara Keshishian, MD, is the CEO of Hyperion Laboratories, A Delaware Corporation.

Conflicts of Interest

The authors declare no conflicts of interest regarding the publication of this paper.

References

[1] de Jong, P.T.V.M. (2021) The Diopter. *Eye*, **35**, 1801-1803. https://doi.org/10.1038/s41433-021-01419-y

[2] Thompson, J.T. and Guyton, D.L. (1983) Ophthalmic Prisms: Measurement Errors and How to Minimize Them. *Ophthalmology*, **90**, 204-210. https://doi.org/10.1016/s0161-6420(83)34572-3

[3] España, E., Alvarez, M.T., Ojea, S. and Keshishian, A. (2025) Measuring Angle of Deviation, Prism Diopter in Children-Assessing Strabismus Using Smartphone Application. *Open Journal of Ophthalmology*, **15**, 132-146. https://doi.org/10.4236/ojoph.2025.153018

[4] Holmes, J.M., Chandler, D.L., Christiansen, S.P., Birch, E.E., Bothun, E., Laby, D., *et al.* (2009) Interobserver Reliability of the Prism and Alternate Cover Test in Children with Esotropia. *Archives of Ophthalmology*, **127**, 59-65.

[5] Freedman, K., Ray, C. and Kirk, D. (2019) Reevaluation of Current Prism Standards with Recommendations to Increase Accuracy in the Measurement of Strabismus. *American Journal of Ophthalmology*, **198**, 130-135. https://doi.org/10.1016/j.ajo.2018.09.009

[6] Lee, L., Feng, K.M., Chuang, P., Chen, Y. and Chien, K. (2023) Preliminary Data on a Novel Smart Glasses System for Measuring the Angle of Deviation in Strabismus. *Eye*, **37**, 2700-2706. https://doi.org/10.1038/s41433-023-02402-5

[7] Cestari, D., Mardiz, G., Bouzika, P., Rajtar, M., Keshishian, A. and Fortin, E. (2018) Evaluation of a Novel Smartphone App for the Automated Strabismus Measurements. https://collections.lib.utah.edu/details?id=1310604&facet_format_t=%22application%2Fpdf%22

[8] Wang, P., Pan, Y., Zhang, J. and Yang, D. (2021) Measurement Errors Induced by Inaccurate Positioning of Ophthalmic Prisms and a Simple Way to Minimize Them. *International Journal of Ophthalmology & Visual Science*, **6**, 59-62. https://doi.org/10.11648/j.ijovs.20210601.19

[9] Rainey, B.B., Schroeder, T.L., Goss, D.A. and Grosvenor, T.P. (1998) Inter-Examiner Repeatability of Heterophoria Tests. *Optometry and Vision Science*, **75**, 719-726. https://doi.org/10.1097/00006324-199810000-00016

[10] Moschos, M.M. (2014) Physiology and Psychology of Vision and Its Disorders: A Review. *Medical Hypothesis, Discovery and Innovation in Ophthalmology*, **3**, 83-90. https://pmc.ncbi.nlm.nih.gov/articles/PMC4348490/

[11] De Nava, A.S.L., Somani, A.N. and Salini, B. (2023) Physiology, Vision. StatPearls. https://www.ncbi.nlm.nih.gov/books/NBK538493/

[12] Solomon, S.G. and Lennie, P. (2007) The Machinery of Colour Vision. *Nature Reviews Neuroscience*, **8**, 276-286. https://doi.org/10.1038/nrn2094

[13] Ichinose, T. and Habib, S. (2022) On and off Signaling Pathways in the Retina and the Visual System. *Frontiers in Ophthalmology*, **2**, Article 989002. https://doi.org/10.3389/fopht.2022.989002

[14] Fox, R.S. and Stern, C. (2023) The Effects of Modulated Light on the Visual Process. *Advances in Ophthalmology and Optometry*, **8**, 15-26. https://doi.org/10.1016/j.yaoo.2023.03.009

[15] Espinosa, J.S. and Stryker, M.P. (2012) Development and Plasticity of the Primary Visual Cortex. *Neuron*, **75**, 230-249. https://doi.org/10.1016/j.neuron.2012.06.009

[16] Qin, W. and Yu, C. (2013) Neural Pathways Conveying Novisual Information to the Visual Cortex. *Neural Plasticity*, **2013**, Article ID: 864920. https://doi.org/10.1155/2013/864920

[17] Choi, R.Y. and Kushner, B.J. (1998) The Accuracy of Experienced Strabismologists Using the Hirschberg and Krimsky Tests. *Ophthalmology*, **105**, 1301-1306.

[18] Alhassan, M., Hovis, J.K. and Chou, R.B. (2015) Repeatability of Associated Phoria Tests. *Optometry and Vision Science*, **92**, 900-907. https://doi.org/10.1097/opx.0000000000000638

[19] Johnson, R., Wynn, S. and Coffey, B. (2004) Influences of Examiner Position and Effective Prism Power on Nearpoint Alternate Cover Test. *Optometry—Journal of the American Optometric Association*, **75**, 496-502. https://doi.org/10.1016/s1529-1839(04)70174-8

[20] Korah, S., Philip, S., Jasper, S., Antonio-Santos, A. and Braganza, A. (2014) Strabismus Surgery before versus after Completion of Amblyopia Therapy in Children. *Cochrane Database of Systematic Reviews*, No. 10, CD009272. https://doi.org/10.1002/14651858.cd009272.pub2

[21] Dembinski, R.L., Collins, M.E. and Kraus, C.L. (2019) Outcomes Following Surgery for Horizontal Strabismus in Children of Lower Socioeconomic Backgrounds. *Strabismus*, **27**, 47-53. https://doi.org/10.1080/09273972.2019.1626451

[22] Cheng, W., Lynn, M.H., Pundlik, S., Almeida, C., Luo, G. and Houston, K. (2021) A Smartphone Ocular Alignment Measurement App in School Screening for Strabismus. *BMC Ophthalmology*, **21**, Article No. 150. https://doi.org/10.1186/s12886-021-01902-w

[23] Pundlik, S., Tomasi, M., Liu, R., Houston, K. and Luo, G. (2019) Development and Preliminary Evaluation of a Smartphone App for Measuring Eye Alignment. *Translational Vision Science & Technology*, **8**, Article 19. https://doi.org/10.1167/tvst.8.1.19

[24] Wang, R., Lyu, J., Yang, Y., Bi, S., Yu, H., Deng, H., *et al.* (2025) A Smartphone-Based Digital Ruler to Automatically Measure Strabismus in Ophthalmologist-Level: A Prospective, Multicenter Cohort Study. *NEJM AI*, **2**, 11. https://doi.org/10.1056/aioa2401205

[25] Bekerman, I., Gottlieb, P. and Vaiman, M. (2014) Variations in Eyeball Diameters of the Healthy Adults. *Journal of Ophthalmology*, **2014**, Article ID: 503645.

https://doi.org/10.1155/2014/503645

[26] Ansari, A.S., Vehof, J., Hammond, C.J., Bremner, F.D. and Williams, K.M. (2021) Evidence That Pupil Size and Reactivity Are Determined More by Your Parents than by Your Environment. *Frontiers in Neurology*, **12**, Article 651755. https://doi.org/10.3389/fneur.2021.651755

[27] Lazar, R., Degen, J., Fiechter, A., Monticelli, A. and Spitschan, M. (2024) Regulation of Pupil Size in Natural Vision across the Human Lifespan. *Royal Society Open Science*, **11**, Article ID: 191613. https://doi.org/10.1098/rsos.191613